Supplementary Material (ESI) for Chemical Communications

Synthesis of Oxygen-Deficient Luminescent Mesoporous Silica Nanoparticles for Synchronous Drug Delivery and Imaging

Qianjun He, Jianlin Shi*, Xiangzhi Cui, Chenyang Wei, Lingxia Zhang, Wei Wu, Wenbo Bu, Hangrong Chen, Huixia Wu

State Key Laboratory of High Performance Ceramics and Superfine Microstructure, Shanghai Institute of Ceramics, Chinese Academy of Sciences, 1295 Ding-Xi Road, Shanghai 200050, China

Experimental

Synthesis of SIC-1

Under argon blowing protection, 1 g of P123 and 2.8 g of NaCl were fully dissolved into 80 mL of HCl solution (2 M) at 25 °C under intensive stirring. Then 1.8 mL of triethoxysilane (TES) was added dropwise under gentle stirring. After 1 hour, the reaction solution in a semi-transparent colloidal state was centrifugated for 10 min with the centrifugal force of 18000*g* in a high speed refrigerated centrifuge. Collected nanoparticles were extracted for several times under ultrasonic assistance with ethanol to remove residual P123. Finally, products were dispersed in super-pure water and the freeze drying power was used for measurements.

Synthesis of SIC-2, SIC-3 and SIC-4

The synthesis procedures of sample SIC-2 were the same to that of sample SIC-1 except no argon blowing protection. The synthesis procedures of sample SIC-3 were also the same to that of sample SIC-1 except no addition of NaCl. Sample SIC-4 was synthesized at an over high sol-gel temperature of 38 °C with other synthesis processes same to sample SIC-1.

Synthesis of SIC-500, SIC-600, SIC-700 and SIC-900

Sample SIC-1 was calcined for 2 hours respectively at 500 °C, 600 °C, 700 °C and 900 °C at a heating rate of 2 °C min^{-1} under nitrogen blowing protection to obtain samples SIC-500, SIC-600, SIC-700 and SIC-900.

Characterization

The morphology and mesostructure of nanoparticles were observed via transmission electron microscopy (TEM) and scanning electron microscopy (SEM), which were performed on a JEM–2010 electron microscope attached with an Oxford Link ISIS energy-dispersive X-ray spectroscopy and a JSM-6700F electron microscope, respectively. Meanwhile, energy dispersive spectra (EDS) were collected on observed nanoparticles, and the ratios of oxygen to silicon of as-synthesized and post-calcined samples were determined. Small-angle and wide-angle X-ray diffraction (SAXRD) data were recorded on a Rigaku D/Max-2550V diffractometer using Cu Kα radiation (40 kV and 40 mA) at a scanning rate of 0.4° min^{-1} over the range of 0.6–60°. The porosity was measured by nitrogen adsorption–desorption isotherm experiments, which were carried out on a Micromeritics Tristar 3000 analyzer at 77 K under a continuous adsorption condition, with all samples were dried for 12 h at 120 °C under nitrogen before measurements. Average pore diameter was calculated from

desorption branches of the nitrogen adsorption–desorption isotherms by the Barrett–Joyner–Halenda (BJH) method, and specific surface area and pore volume were calculated by Brunauer–Emmett–Teller (BET) and BJH methods, respectively. Luminescent spectra of sample aqueous solutions excitated at 278 nm were detected under the same experimental conditions using a Shimadzu RF-5301 Spectrofluorophotometer with a xenon lamp. The thermal decomposition process of sample SIC-1 was measured by a TG thermal analyzer over the range of 30–600 ºC at a heating rate of 5 °C min^{-1} in nitrogen. To determine the ratios of oxygen to silicon of as-synthesized and post-calcined samples and the oxidation states of silicon, X-ray photoelectron spectroscopy (XPS) were collected on a VG Micro MKII instrument using monochromatic Al Ka X-rays, and the spectrum calibration was performed by taking the C 1s electron peak (285 eV) as the internal reference. All samples were adequately dewatered in ultra-high vacuum before XPS measurements. FTIR spectra were collected on a Nicolet (Madison, WI) Magna 550 infrared spectrophotometer using KBr technique. Three hundred scans were collected per sample over the range of 2500 to 400 cm^{-1} at a resolution of 4 cm^{-1}.

Cytotoxicity of the cargo SIC-600 against normal cells

Two representative normal cells, human embryonic kidney 293 cells and fibroblast L929 cells, were respectively cultured in the DMEM culture medium containing 10% fetal bovine serum (FBS). All cells were maintained at 37 °C in a humidified and 5% CO_2 incubator. For all experiments, cells were harvested by the use of D-Hank's-trypsin solution and resuspended in fresh medium before plating. In vitro cytotoxicity was assessed by the standard Cell Counting Kit-8 (CCK-8) assay. The statistical evaluation of data was performed using a two-tailed unpaired Student's *t*-test. A p-value of less than 0.05 was considered statistically significant. Each data point is represented as mean ± standard deviation (SD) of eight independent experiments ($n = 8$, n indicates the number of wells in a plate for each experimental condition). The dose dependence of the cytotoxicity was investigated at different particle concentrations (3.1–100 $\mu g \cdot mL^{-1}$).

Cells were seeded in 96-well plates at a density of 2×10^4 cells per well. After incubation for 24 h at 37 °C in 100 μL culture medium containing 10% FBS, culture medium was discarded and then cells were treated with 100 μL pH 7.4 D-Hank's solution of samples at different concentrations. After incubation for 24 h, 10 μL of CCK-8 solution was added. After another 4 h, the absorbance was monitored at 450 nm on a micro-plate reader (Bio-Tek ELx800). A culture medium without the addition of nanoparticles was used as the blank control. A culture medium with the addition of nanoparticles at corresponding concentrations but no addition of CCK-8 solution was used as the background needing to be subtracted for eliminating the luminescent interference of samples. The cytotoxicity was expressed as the percentage of the cell viability as compared with the blank control.

Drug loading, intracellular delivery, cytotoxicity against cancer cells and live cell imaging

The optimal sample SIC-600 was used to load/deliver an anticancer drug doxorubicin (DOX) to kill cancer cells (MCF-7 and BT-474 cells) and luminescently image these cells. As for drug loading, sample SIC-600 was firstly dried for 12 h at 120 °C in vacuum, and then further kept in vacuum at room temperature for 3 h. Then the aqueous solution of DOX (10 mg mL^{-1}) was added into dry sample SIC-600, and then stabilized at room temperature for 1 hour. Finally, DOX-loaded SIC-600

nanoparticles were collected by centrifugation, and dried in vacuum. According to the difference between UV adsorbances of DOX solutions before and after loading (Shimadzu UV-3101PC UV-vis absorption spectrophotometer), the drug loading capacity of SIC-600 was calculated to be 128 mg · g^{-1} by the Beer–Lambert law.

MCF-7 cells were cultured in the RPMI 1640 culture medium containing 10% fetal bovine serum (FBS). BT-474 cells were cultured in the ATCC Hybri-Care culture medium containing 10% FBS. Cytotoxicity of loaded-DOX SIC-600 against MCF-7 and BT-474 cells was measured as above-mentioned CCK-8 assay. Meanwhile, some cells prior to the treatment with CCK-8 solution were washed for several times with D-Hank's solution to remove the residual nanoparticles, and then directly observed for the intracellular internalization and drug delivery of DOX-loaded SIC-600 under an Olympus FV1000-IX81 confocal microscopy.

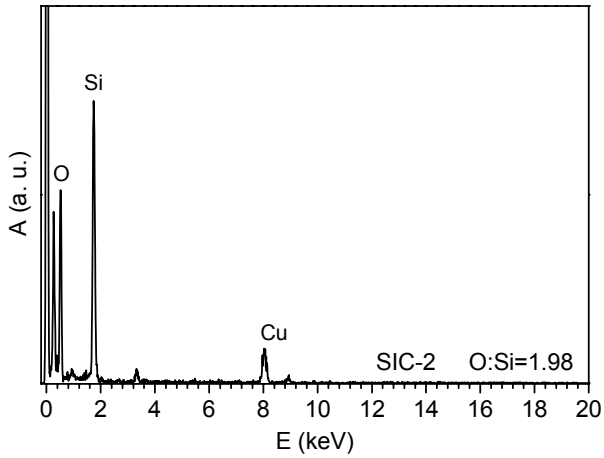

Figure S1. EDS spectrum of the sample SIC-2 synthesized in air without inert atmosphere protection. The molar ratio of oxygen to silicon is calculated to be about 1.98, suggesting that sample SIC-2 had been oxidized into silica and therefore cannot be induced to generate luminescence.

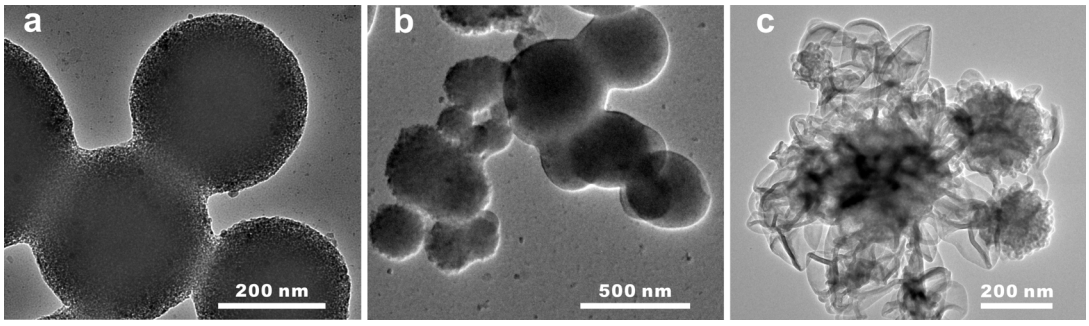

Figure S2. TEM images of samples SIC-3, SIC-4 and SIC-700 synthesized without the addition of inorganic salt, at an over high sol-gel temperature of 38 °C, and at an over high post-calcination temperature of 700 °C, respectively. Nanoparticles in sample SIC-3 easily conglomerate with each other without the addition of inorganic salt playing a phase separation role. Nanoparticles in sample SIC-4 are also subject to conglomerating with each other, and their particle sizes are much non-uniform, probably because of fast hydrolysis and condensation of silicon source at an over high sol-gel temperature of 38 °C. After sample SIC-1 was post-calcined for 2 hours at an over high post-calcination temperature of 700 °C, a kind of large nano-flakes was formed of sample SIC-700 and the initial mesoporous structure collapsed.

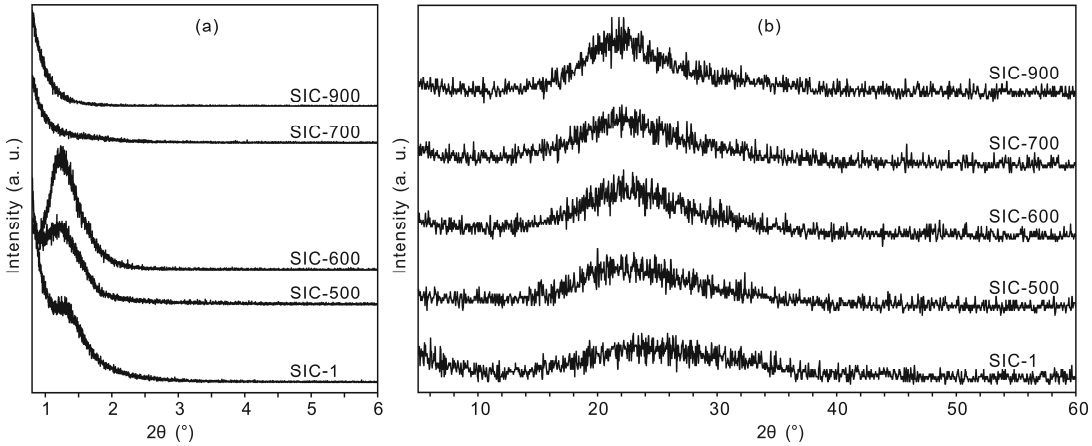

Figure S3. Small-angle (a) and wide-angle (b) XRD patterns of the as-synthesized sample SIC-1, and the post-calcined samples SIC-500, SIC-600, SIC-700 and SIC-900.

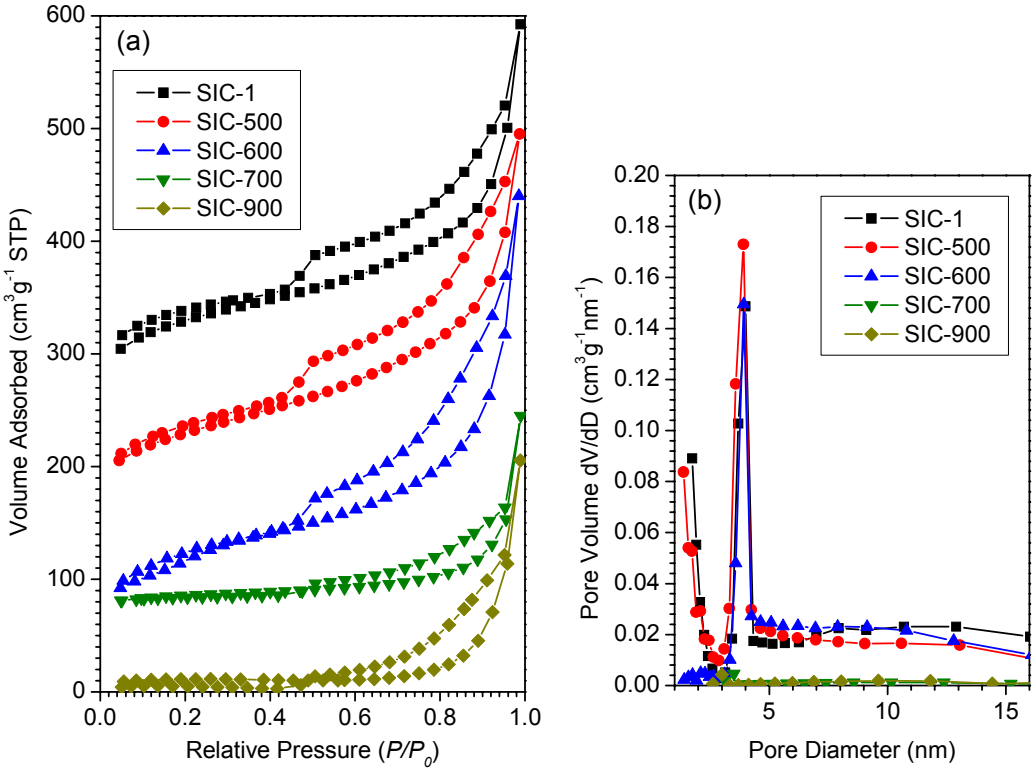

Figure S4. Nitrogen adsorption–desorption isotherms (a) and pore size distribution curves (b) of samples SIC-1, SIC-500, SIC-600, SIC-700 and SIC-900. BET specific surface areas of samples SIC-1, SIC-500, SIC-600, SIC-700 and SIC-900 were calculated to be 410, 360, 356, 62 and 56 $m^2 \cdot g^{-1}$. Pore volumes of samples SIC-1, SIC-500, SIC-600, SIC-700 and SIC-900 were calculated to be 0.53, 0.54, 0.56, 0.27 and 0.3 $cm^3 \cdot g^{-1}$. Samples SIC-1, SIC-500 and SIC-600 have the almost same most probable pore size of about 4 nm, however both samples SIC-700 and SIC-900 have no distinct mesopore.

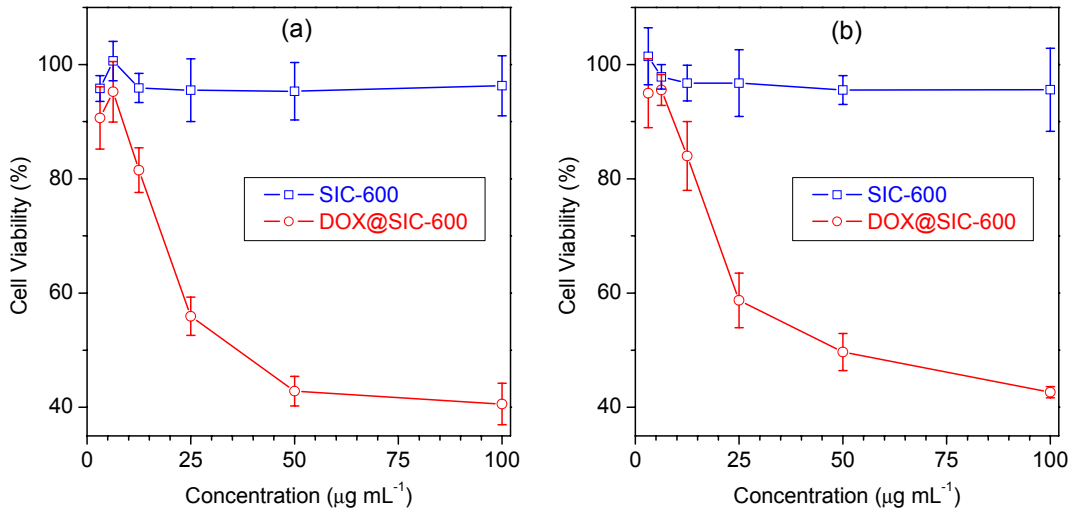

Figure S5. Cytotoxicity of the cargo SIC-600 and the DOX-loaded SIC-600 against MCF-7 cells (a) and BT-474 cells (b).

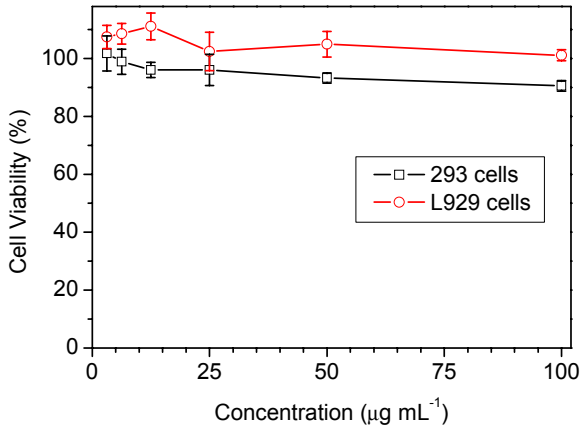

Figure S6. Cytotoxicity of sample SIC-600 against 293 and L929 cells.

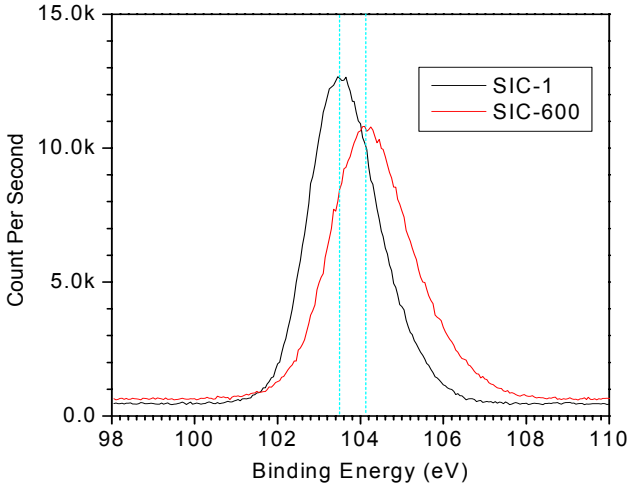

Figure S7. High-resolution XPS spectra in the Si 2p spectral region of samples SIC-1 and SIC-600. Compared with sample SIC-1 (103.5 eV), sample SIC-600 shows a higher Si 2p binding energy of 104.1 eV, which could be resulted from the condensed network during post-calcination as evidenced by the blue shift of the Si–O–Si FTIR stretching bands at 1000−1300 cm^{-1} (Fig. S10). [1]

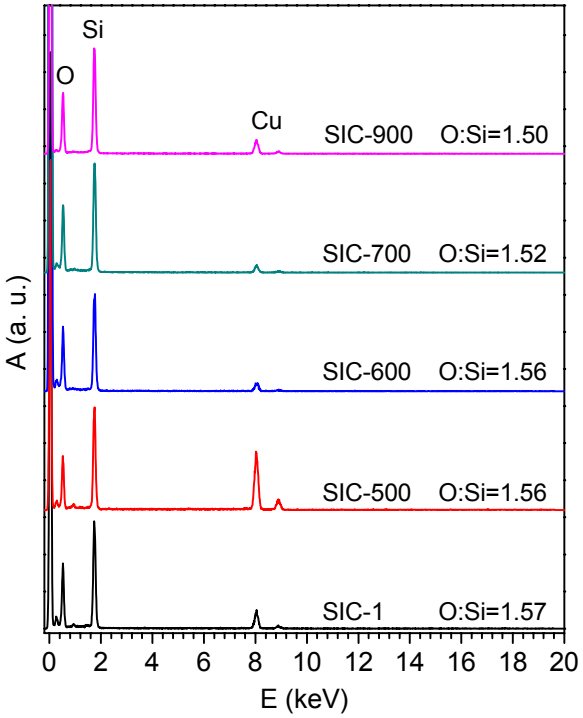

Figure S8. EDS spectra of the as-synthesized sample SIC-1 and the post-calcined samples SIC-500, SIC-600, SIC-700 and SIC-900.

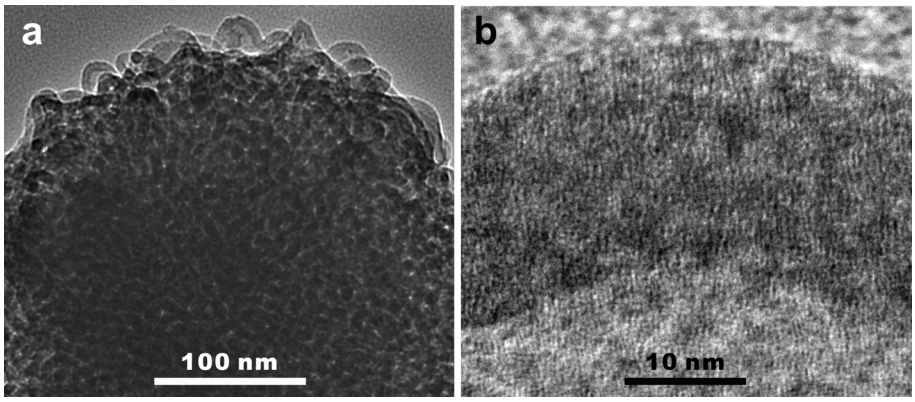

Figure S9. High-magnification TEM images of sample SIC-600. No observable crystal lattice fringe of silicon indicates that no definite silicon crystalline phase was generated during post-calcinatioin.

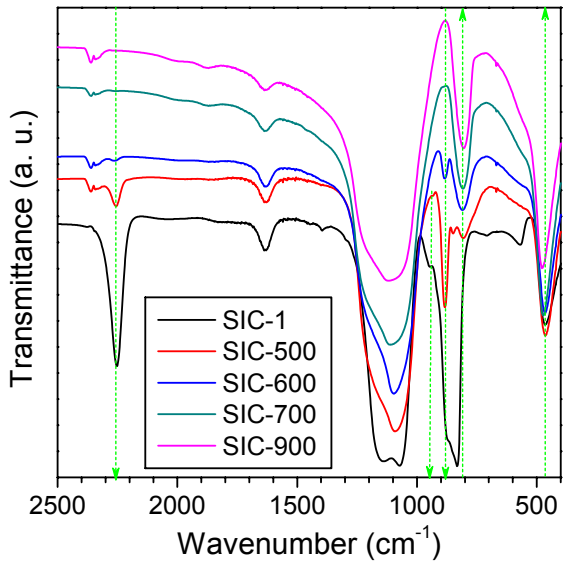

Figure S10. FTIR spectra of the as-synthesized sample SIC-1 and the post-calcined samples SIC-500, SIC-600, SIC-700 and SIC-900. Sample SIC-1 shows two characteristic absorption bands of $O_3Si{-}H$ at 2252 cm^{-1} and 883 cm^{-1}, which are readily assigned to Si−H stretching and bending vibrations, respectively [2]. With the increase of calcination temperature, both peaks became gradually weaker and finally disappeared, indicating the breakdown of Si−H bond. In addition, the 883 cm^{-1} band disappearance is also associated with the formation of sub-oxidized silicon species containing Si–Si bonds [3]. Furthermore, sample SIC-1 shows a weak absorption band at 964 cm^{-1}, which should be attributed to the Si−OH stretching of free silanols. After calcinations for 2 hours above 500 °C, this Si−OH band disappeared, indicating that the Si–O–Si network was contracted by the dehydration between Si−OH groups. Meanwhile, three absorption bands around 460 cm^{-1}, 806 cm^{-1} and 1090 cm^{-1}, respectively related to the rocking, bending and internal TO (transverse optic) stretching vibrations of Si–O–Si, became stronger as compared with the external LO (longitudinal optic) stretching vibration around 1145 cm^{-1}, and the composite Si–O–Si stretching band at 1000−1300 cm^{-1} was broadened, which suggests that the Si–O–Si network became more disordered because of the formation of O3Si–SiO3 bond derived from the Si−H rupture [4,5].

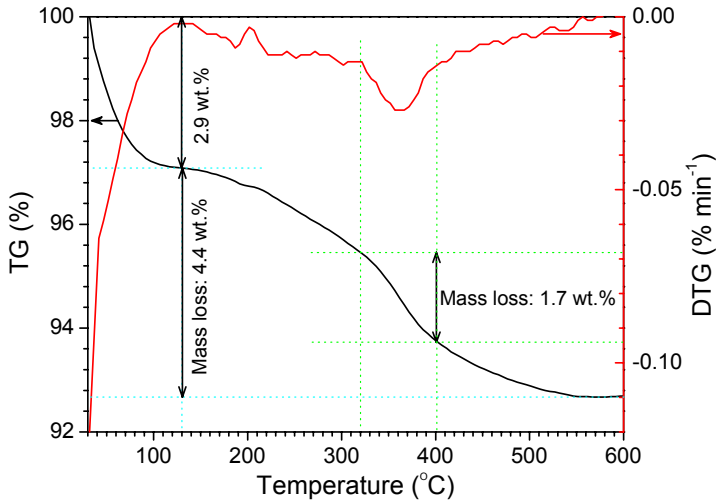

Figure S11. TG/DTG curves of the as-synthesized sample SIC-1. The dehydrogenization between $O_3Si{-}H$ terminal groups and the dehydration between Si−OH groups during post-calcination can also be inferred from a continuous mass loss of 4.4 wt.% between 130 °C and 600 °C. Especially, a sharp mass loss of 1.7 wt.% between 320 °C and 400 °C strongly suggests a fast dehydrogenization stage.

References

[1] H. J. Li, H. H. Sun, X. C. Tie and X. J. Xiao, *Sci*. *China Ser*. *E-Tech*. *Sci*., 2008, **51**, 113.
[2] C. M. Hessel, E. J. Henderson and J. G. C. Veinot, *Chem*. *Mater*., 2006, **18**, 6139.
[3] J. A. Luna-López, G. García-Salgado, T. Díaz-Becerril, J. Carrillo López, D. E. Vázquez-Valerdi, H. Juárez-Santiesteban, E. Rosendo-Andrés and A. Coyopol, *Mater*. *Sci*. *Eng*. *B*, 2010, **174**, 88.
[4] R. S. Brusa, W. Deng, G. P. Karwasz, A. Zecca, G. Mariotto, P. Folegati, R. Ferragut and A. Dupasquier, *Appl*. *Surface Sci*. 2002, **194**, 106.
[5] D. Nesheva, I. Bineva, Z. Levi, Z. Aneva, Ts. Merdzhanova and J. C. Pivin, *Vacuum*, 2003, **68**, 1.